Modeling surface climate in US cities using Simple Biosphere model SiB2

Ping Zhang[1,2], Lahouari Bounoua[1], Kurtis Thome[1], Robert Wolfe[3], Marc Imhoff[2]

[1] Biospheric Sciences Laboratory, NASA's Goddard Space Flight Center, Greenbelt, MD, 20771, USA

[2] Earth System Science Interdisciplinary Center, University of Maryland, College Park, MD 20742, USA

[3] Terrestrial Information Systems Laboratory, NASA's Goddard Space Flight Center, Greenbelt, MD, 20771, USA

Send correspondence to:

Ping Zhang

Biospheric Sciences Laboratory Code 618

NASA's Goddard Space Flight Center

Greenbelt, MD, 20771, USA

Tel.: 301-614-6698

Fax: 301-614-6695

Ping.Zhang@nasa.gov

Prepared for the

Canadian Journal of Remote Sensing

Abstract (100-200 word)

We combine Landsat- and the Moderate Resolution Imaging Spectroradiometer (MODIS)-based products in the Simple Biosphere model (SiB2) to assess the effects of urbanized land on the continental US (CONUS) surface climate. Using National Land Cover Database (NLCD) Impervious Surface Area (ISA), we define more than 300 urban settlements and their surrounding suburban and rural areas over the CONUS.

The SiB2 modeled Gross Primary Production (GPP) over the CONUS of 7.10 PgC (1 PgC= 10^{15} grams of Carbon) is comparable to the MODIS improved GPP of 6.29 PgC. At state level, SiB2 GPP is highly correlated with MODIS GPP with a correlation coefficient of 0.94. An increasing horizontal GPP gradient is shown from the urban out to the rural area, with, on average, rural areas fixing 30% more GPP than urbans. Cities built in forested biomes have stronger UHI magnitude than those built in short vegetation with low biomass. Mediterranean climate cities have a stronger UHI in wet season than dry season. Our results also show that for urban areas built within forests, 39% of the precipitation is discharged as surface runoff during summer versus 23% in rural areas.

1. Introduction

Although urban areas cover less than 1% of the world's surface, more than 50% of the world population now lives in urban areas (Schneider et al., 2010; UN2008). The process of urbanization has strong impacts on ecosystems' functions, human health, local weather and possibly surface climate through various physical land surface changes. One of the major impacts of urbanization is the complete loss of activity resulting from permanently replacing fertile lands by impervious surfaces (Bounoua et al, 2009; Imhoff et al., 2004; Qureshi, 2010). Urban land transformation in the US has reduced the amount of net carbon fixed through photosynthesis by 0.04 pg per year or 1.6% of the pre-urban input (Imhoff et al., 2004). A Case study (Zhang et al., 2012) shows that about 0.21 Pg carbon is lost in Southern United States due to urban land conversion between 1945 and 2007. The initial carbon loss due to land conversion may be compensated for after 70-100 years once planted trees and lawns in the urban ecosystem gradually accumulates carbon (Zhang et al., 2012).

The urban heat island (UHI) effect is another significant consequence of urbanization. The UHI phenomenon is generally seen as being caused by a reduction in latent heat flux and an increase in sensible heat in urban cores as evaporating vegetated lands are replaced by impervious relatively low albedo pavement and building materials (Bounoua et al., 2015). This creates a difference in surface temperature between urban and surrounding non-urban areas (e.g.; Quattrochi and Ridd 1994; Grimmond and Oak 2002; Shepherd and Burian 2003).

In general, the UHI, as measured by air temperature, is most evident on a clear and windless night with peaks in the late evening to early morning hours (Kim and Baik 2002). Arid urban areas, however show a relatively weak UHI and sometimes even an urban heat sink as a result of the prevalence of irrigated lawns and exotic trees within the urban areas (Diem and Brown 2003,

Imhoff et al., 2010, Shepherd, 2005 and 2006). The urban heat island phenomenon can also be characterized by land surface (skin) temperatures (LST). While LST can be both higher and spatially more variable than corresponding air temperatures due to the surface cover heterogeneity and complexity (e.g. Nichol 1996, Streutker 2002), they are more closely dependent on surface conditions (Owen et al. 1998, Nichol and Wong 2005, Voogt and Oke 2003). Since surfaces heat up and cool faster than air, the greatest surface temperatures (LSTs) in urban centers are observed around midday versus nighttime for air temperature (Roth et al. 1989).

Increased impervious surface area associated with urbanization also affects the natural cycling of water. Urbanization can impact precipitation or convection by increasing surface roughness (e.g., Bornstein and Lin, 2000), enhancing aerosols for cloud condensation nuclei sources (e.g. Diem and Brown, 2003), and UHI-generated convective clouds (Shepherd and Burian 2003, Shepherd 2005). At the same time, urbanization also changes hydrological processes within watersheds by reducing surface infiltration and altering the base flow, increasing peak discharge and surface runoff (Dougherty et al., 2006; Du et al., 2012, and Miller et al., 2014, Bounoua et al., 2015.a).

In this paper we use the Landsat-based ISA from the National Land Cover Dataset (NLCD) (Homer et al., 2004) to characterize the urban areas, and MODIS-based biophysical products at 8-days interval (Bounoua et al, 2015.b) to describe the vegetation phenology within a Climate Modeling Grid (CMG) of 0.05° x 0.05° of latitude-longitude to simulate the impact of urbanization as a form of land use on the continental US (referred as CONUS in the rest of the paper) surface carbon, energy and water cycles for the year 2001. To do so, we use the Simple Biosphere model (SiB2) of Sellers et al. (1996) as modified by Bounoua et al. (2009) to describe the physical processes associated with urbanization.

2. Methods and Data

2.1 Land Cover and Biophysical Parameters

Impervious Surface Area from the NLCD was used to characterize urban land cover (LC) for the year 2001. The fractional ISA of the NLCD were retrieved from Landsat 7 Enhanced Thematic Mapper Plus and IKONOS discriminating man-made surfaces from natural or vegetated lands (Homer et al. 2004). The ISA data was combined with MODIS collection 5 land cover (MCD12Q1) for the year 2001. The MODIS MCD12Q1-Type 1 (IGBP) land cover classification has 17 distinct cover types including a build-up (Hansen et al., 2000). We retain the percentage of Landsat ISA and proportionally distributed the difference between NLCD ISA and MODIS build-ups over other non-impervious LC types co-existing in the CMG. The final product provides a 2001 land cover gridded map where grid cells may include ISA fractions from Landsat and fractions from all MODIS land cover types co-existing in the same CMG (Bounoua et al, 2015).

Additionally, a set of biophysical parameters required for the LSM was generated using the MODIS 500m land cover map and the 500m, 8-day composite gap-filled Normalized Difference Vegetation Index (NDVI) developed for the North American Carbon Program (NACP) (Tan et al. 2011). In each CMG, the NDVI was averaged over each of the existing LC type. NDVI estimates for impervious surfaces were generated using Landsat data. The biophysical parameters include the fraction of the Photosynthetically Active Radiation (fPAR) absorbed by the green vegetation canopy, the Leaf Area Index (LAI), the Greenness fraction (G), the canopy roughness length (Z_0) and the canopy zero-plane displacement (d) for different land cover types.

2.2 The Land Surface Model

The Simple Biosphere model SiB2 of Sellers et al. (1996) as modified by Bounoua et al. (2009) is used in this study. SiB2 is a biophysically based land surface model that computes the exchanges of carbon, energy, water, and momentum between the land surface and the atmosphere, accounting for 12 distinct vegetation classes (Sellers et al., 1996). The drivers of the model include short- and longwave radiation, large-scale and convective precipitation rates, and the temperature and wind speed at a reference level above the canopy. These meteorological drivers for the year 2001 are obtained from the Phase 2 of the North American Land Data Assimilation System (NLDAS-2) [Mitchel et al. 2004].

2.3. MODIS Gross Primary Production (GPP) and Land Surface Temperature (LST)

We compare the SiB2 modeled land surface temperature with MODIS-Terra Version 5, 8-day (MOD11A2) LST with high quality control (Wan et al., 2004). LST's from MODIS are retrieved from clear-sky (99% confidence) observations at day time and night time using a generalized split-window algorithm (Wan and Dozier 1996). Comparisons between MODIS LST's and in-situ measurements across a wide set of test sites indicate an accuracy better than 1°C with a root mean square error RMS (of differences) less than 0.5 °C in most cases (Wan 2008, Wang et al. 2008).

In our comparisons, we also used the improved 1km MODIS gross primary production (GPP) with high quality control (Zhao et al. 2006, 2010) to compare to the SiB2 predicted GPP. MODIS GPP is calculated through the BIOME-BGC model using satellite-derived land cover, fraction of photosynthetically active radiation (FPAR), and leaf area index (LAI) as input surface vegetation information (Zhao et. al 2006.). The MODIS GPP datasets was obtained from the

Numerical Terradynamic Simulation Group, School of Forestry, University of Montana (http://www.ntsg.umt.edu/).

2.4. Sampling urban areas over USA

We use the Landsat-derived National Land Cover Database ISA for 2001 (Xian et al., 2011) to define more than 300 cities with an area larger than 10 km^2 over the CONUS. This ISA dataset characterizes the CONUS urban development as function of the extent and spatial distribution of a collection of man-made surfaces within a pixel (e.g.; Yang et al., 2002, Fry et al., 2011, Xian et al., 2011). We use a 25% ISA threshold to define the boundary of urban and suburban zones (Imhoff et al. 2010; Zhang et al., 2010 and 2012) with urban areas having more than 25% ISA. A 5km width buffer zone adjacent to and outside the 25% ISA contour defines the immediate surrounding suburban area, and a second 5km width buffer zone located 15km to 20km away from the 25% ISA contour is defined as the rural zone. We use the terrestrial ecoregion map of Olson et al. (2001) to group 300+ US cities into four major biomes: forest, grassland, desert, and Mediterranean, each representing an assemblage of biophysical, climate, botanical and animal habitat characteristics of a distinct geographical area.

3. Results

3.1 Gross Primary Production (GPP)

We obtained the annual SiB2 modeled GPP over the CONUS by adding monthly GPP for each land cover class weighted by its fraction. The modeled total GPP is 7.10 PgC (1 PgC= 10^{15} grams of Carbon). This total is closely comparable to the MODIS improved CONUS annual GPP (Zhao and Running, 2010) of 6.29 PgC during 2001. Figure 1 shows the spatial distribution of the annual GPP over CONUS calculated from MODIS-algorithm and SiB2 model. Both GPP

maps show close agreement at regional scale: high carbon uptake is found in forested regions especially in the southeast. Low carbon uptake is found in the arid and semi-arid regions where the vegetation growth is limited by water availability; and in mountains where vegetation growth is constrained by low temperatures. However, MODIS improved GPP is missing most of the urban cores whereas SiB2 model, with its sub-grid land cover characterization, is capable to identify urban vegetation and captures some GPP in urban cores. For all US land area, excluding water, croplands cover about 32.1% and account for 38.55% of the annual GPP, ranking as the primary land cover type in carbon uptake (Table 1). Grasslands rank the second in terms of area and GPP. The impervious surface areas cover 1.06% of the total land in the CONUS and uptake 0.003 PgC or 0.04% of the total GPP. Even though in term of area, ISA covers a small fraction of land, its estimated impact on the carbon uptake is not negligible. For example, if all the ISA is replaced by evergreen broadleaf forest, the estimated carbon uptake over the CONUS will increase by 0.13 Pg. The numbers from MODIS improved GPP are similar and are shown in Table 1.

Overlaying the state's boundaries over the GPP maps, we estimated the total GPP for each state in the CONUS. We show a strong linear relationship, correlation coefficient of 0.94, between SiB2 GPP and MODIS improved GPP (Figure 2). At this spatial scale, on average, SiB2 GPP is about 11% larger than that of MODIS. Both GPP maps show Texas has the most annual GPP, followed by California. On the other hand Delaware, Rhode Island, and the District of Columbia have the least annual GPP.

Using the spatial distribution of the NLCD ISA and the annual GPP, we define more than 300 cities over the CONUS with areas larger than 10 km^2. Further grouping following the ecological map led to 180 cities built in forests, 90 in grasslands, 8 in a Mediterranean biome, and 29 in arid

and semi-arid biomes. Figure 3 shows the average annual GPP for each ecological grouping. As expected, SiB2 simulated higher GPP for cities embedded within forest biomes, followed by those urban areas built in short vegetation such as grasslands. Low GPP is simulated in desert regions with limited water availability. Within the same biome, the average annual GPP in the rural area is larger than that of the suburban, itself larger than that of the urban area. For example, in the forested biome, the average rate of carbon uptake is about 1028 gC/m^2 in the urban area, 1256 gC/m^2 in suburban area, and 1340 gC/m^2 in the rural area. The process of urbanization, replacing the natural vegetation with impervious surface areas, creates a horizontal GPP gradient between the urban and the rural areas. On average, rural zones fix about 30% more GPP than the urban areas.

3.2 Surface temperature and surface Urban Heat Island (SUHI)

SiB2 model predicts three temperatures: canopy, ground, and deep soil temperatures (Sellers et al. 1996). In this analysis, we use both the canopy and the ground temperatures to examine the temperature difference between ISA and other vegetated land cover types, and the SUHI of cities built in different biomes, defined as the surface temperature difference between the urban core, fully impervious, and the surrounding vegetated lands. The SUHI is different from the UHI obtained from air temperature (Roth et al. 1989).

To do so, we calculate the weighted surface temperature of all the CMGs that have both ISA (>1%) and other vegetated land covers. Excluding inland water, ISA accounts for 6% of all these CMGs (with ISA>1%) and the other vegetated land cover types account for 94%. Figure 4 shows the spatial distribution of ISA and within-CMG summer (June-July-August) temperature difference between the ISA and the fraction-weighted vegetated cover types co-existing in the

CMG. In general, the ISA is warmer than the vegetated land cover in most of the CONUS. Cities in high latitudes tend to show larger temperature differences than those in low latitudes. This is partially due to the fact that the cooling effect of the vegetation is decreased in warmer climate when vegetation experiences a high temperature stress and scales down its photosynthetic activity (Bounoua et al., 2009). Our results also show that the ISA in CMGs located in arid and semi-arid regions have smaller temperature differences; and sometimes the non-urban land cover is warmer than the ISA, generating a Surface Urban Heat sink (SUHS). The reversal in horizontal surface temperature gradient in these arid cities, such as Phoenix and Las Vegas is due to introduction in urban areas of exotic trees and lawns maintained by irrigation and fertilization (Imhoff et al., 2010). In these mostly bare CMGs, the bare soils behave like the ISA, most of the absorbed solar energy is restored as sensible heat flux, reducing thus the horizontal temperature gradient between ISA and non-urban cover (Bounoua et al., 2009). Figure 5 illustrates the annual cycle of monthly average surface temperature for ISA and vegetated lands, as well as their difference. The ISA has a peak monthly mean surface temperature around 27.9 ^{o}C in August and a minimum around 1.6 ^{o}C in January. By contrast, the weighted surface temperature for all vegetated land covers reaches a maximum of 26.1 ^{o}C in August and a minimum of 0.2 ^{o}C in January. Over the CONUS, this surface temperature difference is larger than 1.5 ^{o}C all year long except for January and November. It is larger than 2 ^{o}C for the months of May and June. This temperature difference between ISA and other vegetated land cover types is not the typical SUHI. However, because it accounts for the entire ISA and land cover fractions over the CONUS, it may be considered as the average impact of ISA on surface temperature in urban areas. This result clearly indicates the continental scale impact of urbanization on the CONUS surface climate, an average monthly mean warming of more than 1.5 ^{o}C.

Using the same 300+ cities, we also calculate the urban heat island using both the ground surface and the canopy temperature simulated by SiB2. As discussed in the previous section, we use the average surface temperature inside the urban boundary as the urban temperature and the average temperature of the 15-20 km buffer as the rural temperature. Figure 6 shows the monthly SUHI and the monthly precipitation for urban areas built in forested and Mediterranean biomes. The magnitude of SUHI from urban areas built within forests is maximum during summer. SUHI generated in cities built within grasslands (not shown) have similar seasonal variations but smaller magnitudes. On the other hand, the UHI generated in cities built in a Mediterranean biome (e.g.; cities in California) is more than 2^{o}C in winter and spring and less than 1^{o}C in summer. This pattern agrees well with the seasonal variations of the monthly precipitation: wet seasons in winter and spring and dry seasons in summer and fall. In general in forested biomes the ground is shaded, especially during the summer when canopy are covered with leaves, and cooler than the exposed canopy and therefore generate a much stronger contrast with the urban ground temperatures. This effect is less visible in cities built in Mediterranean biome where trees are sparse and the ground is exposed. In the latter case the ground-based SUHI is similar to the canopy generated SUHI during the fall through spring, but much less during summer.

We compared the average summer (June-July-August) SUHI in the 300+ cities using different temperature products including SiB2 modeled ground and canopy temperatures, and MODIS Terra 8-day land surface temperature (SiB2 modeled LSTs are calculated based on monthly mean outputs and the SUHI reflects the temperature difference between urban and surrounding rural areas for the season. By contrast, MODIS-Terra LSTs are calculated as the average of daytime (10:30) and nighttime (22:30) measurements; monthly mean SUHI are then estimated using these 8 day LSTs. Table 2 shows for cities built in forest, SiB2 simulates an average

summer UHI between the urban core and surrounding rural area, 15-20 km away from the urban, of 0.91 ^{o}C when using ground temperature and 0.62 ^{o}C when using canopy temperature. When using the LST from MODIS we estimate a much larger SUHI of 3.58 ^{o}C. For cities built in other biomes, the results are similar but with smaller magnitude. In high biomass forested biomes, urban areas are surrounded by dense and tall vegetation which intercepts and re-evaporates precipitation at potential rates and diffuses water from the root zone to the atmosphere during the process of photosynthesis, thus keeping the surrounding regions much cooler than the less vegetated urban core. In contrast, urban areas dominated by shorter, less dense, vegetation such as grassland produce a weaker SUHI. In these regions, the zones surrounding the urban core are sparsely vegetated and restore an important part of the absorbed solar energy as sensible heating; thus reducing the horizontal temperature gradient between the urban and surrounding rural areas.

3.3 Precipitation and Surface Runoff

In SiB2, the precipitation is distributed into canopy interception and throughfall components. Canopy interception either evaporates at the potential rate or contributes to throughfall when the canopy holding capacity is exceeded. The combined canopy water is added to the ground liquid water store from which it either evaporates or infiltrates into a shallow surface layer (2cm for all vegetated lands and 2mm in impervious surfaces) if the ground storage capacity is reached. When the infiltration rate is higher than the soil infiltration capacity, the excess water contributes to surface runoff (Bounoua et al, 2009).

We calculated the seasonal precipitation and surface runoff for the same 300+ cities over the CONUS grouped within the four major biomes described above. We first calculated the monthly precipitation for each urban area limited by a 25% ISA contour, and for the surrounding rural

area located within a 5km wide ring 15 km away from the 25% ISA contour. Given the satellite measured land cover composition and the SiB2 modeled surface runoff for each land cover type within each CMG, we estimate the incoming seasonal average precipitation, the fraction-weighted seasonal average surface runoff (the runoff from each LC weighted by its fraction within the CMG) and the ratio of surface runoff to precipitation for each of the 300+ cities and their corresponding rural areas. We then grouped the cities into the four biomes. Table 3 shows that for cities built within forested areas, precipitation has a strong seasonal variation ranging from about 63mm in winter (December-January-February) to about 118 mm in summer (June-July-August). In contrast, in cities built in grasslands and desert areas, precipitation has less seasonal variation with the magnitude of precipitation in desert areas less than half of that in forest. The precipitation seasonal cycle in cities built in the Mediterranean ecoregion is in opposition of phase with that of cities built in forested regions, with the maximum precipitation occurring in winter (81mm) and the minimum in summer (6mm). The precipitation is almost evenly distributed between the urban area and its surrounding rural area in each biome.

For cities built in forest, 39% of the precipitation is expelled as surface runoff during summer in the urban area versus 23% in the rural areas. Cities built in grasslands show that about 70% of the incoming precipitation is discharged as surface runoff in urban area versus 49% in rural area. Mediterranean cities have the most precipitation in winter and expel 69% of it as urban surface runoff versus only 17% in rural areas, whereas, during the season of maximum precipitation, cities built in arid and semi-arid regions (desert) expel about 30% of precipitation as surface runoff in the urban area versus 14% outside of it. In general, vegetation canopy reduces surface runoff by intercepting precipitation on leaves and barks which re-evaporates at potential rates and by holding and using water in the root layer. By contrast, the impervious surface area

strongly reduces the infiltration of water into the ground and because of lack of vegetation it significantly increases the surface runoff. In our study, the urban area and its surrounding rural zone contain a mix of impervious and vegetated surfaces. The relatively high ISA in urban areas results in a large surface runoff to precipitation ratio compared to the more vegetated rural areas. Considering precipitation is evenly distributed between the urban and surrounding rural area, this ratio could be used to inform about the distribution of surface runoff given a rainfall prediction event. This ratio may also be used in designing cities with specific LC elements arrangement that will produce a desired surface water distribution (Bounoua et al., 2015).

The canopy water holding capacity is affected by the seasonal variation in canopy structure, such as the leaf area index (Link et al, 2004). As deciduous leaves drop during winter, canopy water holding capacity decreases and surface runoff increases. Figure 7 shows the SiB2 modeled canopy water holding averaged over urban, suburban, and rural area within the four major biomes. In general, dense tall canopies, such as forest and trees in the Mediterranean ecoregions, have larger water storage than sparse short canopies in grasslands and the deserts. In vegetated biomes, canopy water storage in the middle of the growing season is more than twice that observed outside of the growing season. By contrast, canopy water holding capacity is less than 0.1mm all year long in the desert biome.

4. Conclusion

We use a biophysically based land surface model, SiB2 to examine the urbanization effect on carbon budget, surface energy, and water over the CONUS.

Over the CONUS, the SiB2 modeled GPP is 7.10 PgC which is comparable to the MODIS improved GPP of 6.29 PgC. MODIS improved GPP is missing most of the urban cores where

SiB2 model is capable to identify some GPP over the urban area. The process of urbanization, replacing the natural vegetation with the impervious surface area, produces the horizontal GPP gradient increasing from the urban area to rural area. Our results show that surrounding rural area can fix 30% more GPP than the urban area.

SiB2 modeled temperatures show strong signal of surface urban heat islands at local (CMG), regional (biome) and continental (CONUS) scales. At local scale, CMG located at high latitudes have larger SUHI than those in low latitudes, which is partially due to the vegetation evaporation cooling decreases in warmer climate under high-temperature stresses. On the other hand at regional scale the difference in surface temperature between ISA and other vegetated land covers is more pronounced in cities built in vegetated biomes, whereas at continental scale urban places are simulated to be warmer than rural areas by about 1.5^{o}C year around. We calculated the summer SUHI of 300+ US cities grouped by four major biomes. Cities built in high biomass forested biomes have stronger UHI magnitude than those built in shorter low biomass biomes. Furthermore, Mediterranean cities have a stronger UHI in wet season than dry season.

We estimate the weighted monthly surface runoff for each urban and its surrounding rural area and show that for cities built within forests, about 39% of the precipitation is expelled as surface runoff during summer (June-July-August) in the urban area versus 23% in rural areas. By contrast, in cities built in grassland this ratio is 70% and 49 % in urban and rural, respectively. Considering precipitation is closely distributed between the urban and surrounding rural area, this ratio is informative about the effect of LC on surface runoff and can be used as an indicator for projecting the distribution of surface runoff given a rainfall prediction event.

Acknowledgment

This work is funded by the NASA Interdisciplinary Research in Earth Science NNH09ZDA001N-IDS (2012). Garik Gutman, program manager.

Reference

Akbari, H., 2002. Shade trees reduce building energy use and CO2 emissions from power plants. *Environmental Pollution*, Vol. 116, S119–S126.

Bornstein, R. and Lin, Q. 2000. Urban heat islands and summertime convective thunderstorms in Atlanta: Three cases studies. *Atmospheric Environment*, Vol. 34, pp. 507–516
Bounoua, L., Zhang, P., Mostovoy, G., Thome, K., et al., Impact of Urbanization on Continental US Surface Climate, Environmental Research Letters, under review.

Bounoua, L., Hall, F. G., Sellers, P. J., Kumar, A., Collatz, G. J., Tucker, C. J., and Imhoff, M. L. 2010. Quantifying the negative feedback of vegetation to greenhouse warming: A modeling approach. *Geophysical Research Letters*, Vol. 37, No. 23, DOI: 10.1029/2010GL045338

Bounoua, L., Collatz, G. J., Los, S. O., Sellers, P. J., Dazlich, D. A., Tucker, C. J. and Randall, D. A. 2000. Sensitivity of climate to changes in NDVI. *Journal of Climate*, Vol. 13, pp. 2277–2292.

Bounoua, L., Collatz, G. J., Sellers, P. J., Randall, D. A., Dazlich, D. A., Los, S. O., ... and Jensen, T. G. 1999. Interactions between vegetation and climate: radiative and physiological effects of doubled atmospheric CO2. *Journal of Climate*, Vol. 12 No. 2, pp. 309-324.

Bounoua, L., Safia, A., Masek, J., Peters-Lidard, C., and Imhoff, M. L. 2009. Impact of urban growth on surface climate: A case study in Oran, Algeria. *Journal of applied meteorology and climatology*, Vol. 48, No. 2, pp. 217-231.

Bounoua L., Zhang, P., Mostovoy,G., et al., 2015a, Impact of urbanization on US surface climate, Environmental Research Letter, in press.

Bounoua, L., Zhang, P. Thome, K. et al., 2015b. Mapping Biophysical Parameters for Land Surface Modeling over the Continental US Using MODIS and Landsat, *Dataset Papers in Science*, vol. 2015, Article ID 564279, DOI:10.1155/2015/564279

Diem, J. E. and Brown, D. P. 2003. Anthropogenic impacts on summer precipitation in central Arizona, U.S.A. *Professional Geographer*. Vol. 55, No. 3, pp. 343–355

Dougherty, M., Dymond, R.L., Grizzard Jr, T.J., Godrej, A.N., Zipper, C.E., and Randolph J. 2006. Quantifying long term hydrologic response in an urbanizing basin, *Journal of Hydrologic Engineering*, Vol. 12, No. 1, pp. 33–41

Du, Jinkang, Qian, L. Rui, H. Zuo, T., Zheng, D., Xu, Y. and Xu, C-Y. 2012. Assessing the effects of urbanization on annual runoff and flood events using an integrated hydrological modeling system for Qinhuai River basin, China. *Journal of Hydrology,* Vol. 464 pp. 127-139.

Fry, J., Xian, G., Jin, S., Dewitz, J., Homer, C., Yang, L., Barnes, C., Herold, N., and Wickham, J., 2011. Completion of the 2006 National Land Cover Database for the Conterminous United States, *Photogrammetric Engineering and Remote Sensing*, Vol. 77, No. 9, pp. 858-864.

Grimmond, C.S.B. and Oke, T.R. 2002, Turbulent heat fluxes in urban areas: observations and a Local-scale Urban Meteorological Parameterization Scheme (LUMPS), *Journal of Applied Meteorology,* Vol. 41, pp. 792-810.

Hansen, M. C., DeFries, R. S., Townshend, J. R. G., and Sohlberg, R. 2000. Global land cover classification at 1 km spatial resolution using a classification tree approach. *International Journal of Remote Sensing*, Vol. 21, pp. 1331– 1364.

Homer, C., Huang, C., Yang, L., Wylie, B., and Coan, M. 2004. Development of a 2001 National Land-Cover Database for the United States. *Photogrammetric Engineering and Remote Sensing*, Vol., 70, No. 7, pp. 829-840

Imhoff, M. L., Bounoua, L., DeFries, R., Lawrence, W. T., Stutzer, D., Tucker, C. J., & Ricketts, T. 2004. The consequences of urban land transformation on net primary productivity in the United States. *Remote Sensing of Environment*, Vol. 89, No. 4, pp. 434-443.

Imhoff, M. L., Zhang, P., Wolfe, R. E., and Bounoua, L. 2010. Remote sensing of the urban heat island effect across biomes in the continental USA. *Remote Sensing of Environment*, Vol. 114, No.3, pp. 504-513.

Kim, Y-H. and J-J. Baik. 2002. Maximum urban heat island intensity in Seoul. *Journal of Applied Meteorology*, Vol. 41, pp.651–659.

Link, T.E. Unsworth, M. and Marks, D. 2004. The dynamics of rainfall interception by a seasonal temperate rainforest. *Agricultural and Forest Meteorology* Vol. 124, No. 3 pp. 171-191.

Mitchell, K.E., et al., 2004: The multi-institution North American Land Data Assimilation System (NLDAS): Utilizing multiple GCIP products and partners in a continental distributed hydrological modeling system. J. Geophys. Res., Vol. 109, D07S90, doi:10.1029/2003JD003823.

Miller, James D., et al. 2014, Assessing the impact of urbanization on storm runoff in a peri-urban catchment using historical change in impervious cover. *Journal of Hydrology,* Vol. 515, pp. 59-70.

Nichol, J. 1996, High-resolution surface temperature patterns related to urban morphology in a tropical city: a satellite-based study. *Journal of Applied Meteorology,* Vol. 35, No. 1, pp.135-146.

Nichol, J. and W.S. Wong, (2005), Modeling urban environmental quality in a tropical city. *Landscape and Urban Planning*, Vol. 73, No. 1, pp.49-58.

Olson, D. M., Dinerstein, E., Wikramanayake, E. D., Burgess, N. D., Powell, G. V. N., Underwood, E. C., D'Amico, J. A., Itoua, I., Strand, H. E., Morrison, J. C., Loucks, C. J., Allnutt, T. F., Ricketts, T. H., Kura, Y., Lamoreux, J. F., Wettengel, W. W., Hedao, P., Kassem, K. R. 2001. Terrestrial ecoregions of the world: a new map of life on Earth. *Bioscience*, Vol. 51, No.11, pp.933-938.

Owen, T.W., T.N. Carlson, R.R. Gillies, 1998. An assessment of satellite remotely-sensed land cover parameters in quantitatively describing the climatic effect of urbanization. *Int. J. Remote Sensing*, Vol. 19, No. 9, pp.1663-1681.

Quattrochi, D, and M K. Ridd, 1994. Measurement of thermal energy properties of common urban surfaces using the thermal infrared multispectral scanner, *International Journal of Remote Sensing*, Vol. 15, No.10, pp.1991-2022.

Qureshi S, 2010. The fast growing megacity Karachi as a frontier of environmental challenges: Urbanization and contemporary urbanism issues. *Journal of Geography and Regional Planning*, Vol. 3, No.11, pp.306–321.

Roth, M., T.R. Oke, and W.J. Emery, 1989. Satellite-derived urban heat islands from three coastal cities and the utilization of such data in urban climatology. *Int. J. Remote Sensing,* Vol. *10,* pp.1699-1720.

Schneider, Annemarie, Mark A. Friedl, and David Potere, 2010. Mapping global urban areas using MODIS 500-m data: New methods and datasets based on 'urban ecoregions'. *Remote Sensing of Environment*, Vol. 114, No.8, pp.1733-1746.

Sellers, P. J., Randall, D. A., Collatz, G. J., Berry, J. A., Field, C. B., Dazlich, D. A., ... & Bounoua, L. 1996. A revised land surface parameterization (SiB2) for atmospheric GCMs. Part I: Model formulation. *Journal of climate*, Vol.9, No.4, pp.676-705.

Shepherd, J. M. 2006. Evidence of urban-induced precipitation variability in arid climate regimes. *Journal of Arid Environments*, Vol. 67, pp.607–628.

Shepherd, J. M. 2005. A review of current investigations of urban-induced rainfall and recommendations for the future. *Earth Interactions*, Vol. 9, No.1, pp.1–27.

Shepherd, J. Marshall, and Steven J. Burian. 2003. Detection of urban-induced rainfall anomalies in a major coastal city. *Earth Interactions*, Vol.7, No.4, pp.1-17.

Streutker, D., 2002. A remote sensing study of the urban heat island of Houston, Texas, *International Journal of remote sensing*, Vol. 23, No.13, pp. 2595-2608.

Tan, B., J.T. Morisette, R.E. Wolfe, F. Gao, G.A. Ederer, J. Nightingale, and J.A. Pedelty. 2011. An enhanced TIMESAT algorithm for estimating vegetation phenology metrics from MODIS data. *IEEE Journal of Selected Topics in Applied Earth Observations and Remote Sensing*, Vol. 4, No.2, pp.361-371.

United Nations Department of Economic and Social Affairs, Population Division, 2008
United Nations Department of Economic and Social Affairs, Population Division
World Urbanization Prospects: The 2007 Revision, United Nations Publications (2008)

Voogt, J.A., Oke, T.R., 2003. Thermal remote sensing of urban climates. *Remote Sensing Environ.* Vol. 86, pp.370–384.

Wan, Z., & Dozier, J. 1996. A generalized split-window algorithm for retrieving land-surface temperature from space. *IEEE Transactions on Geoscience & Remote Sensing*, Vol. 34, No.4, pp.892-905.

Wan, Z., Zhang, Y., Zhang, Q., & Li. Z-L. 2004. Quality assessment and validation of the MODIS land surface temperature. *International Journal of Remote Sensing*, Vol.25, pp.261-274.

Wan, Z. 2008. New refinements and validation of the MODIS land-surface temperature/emissivity products. *Remote Sensing of Environment*, Vol.112, pp.59−74.

Wang W., Liang S., & Meyers, T. 2008. Validating MODIS land surface temperature products using long-term nighttime ground measurements. *Remote Sensing of Environment*, Vol.112, No.3, pp.623-635.

Xian, G., Homer, C., Dewitz, J., Fry, J., Hossain, N., and Wickham, J., 2011. The change of impervious surface area between 2001 and 2006 in the conterminous United States. *Photogrammetric Engineering and Remote Sensing*, Vol. 77, No.8, pp.758-762.

Yang, L., Huang, C., Homer, C., Wylie, B., & Coan. M. 2002. An approach for mapping large-area impervious surfaces: Synergistic use of Landsat 7 ETM+ and high spatial resolution imagery. *Canadian Journal of Remote Sensing*, Vol.29, No.2, pp.230-240.

Zhang C, Tian H, Chen G et al (2012) Impacts of urbanization on carbon balance in terrestrial ecosystems of the Southern United States. Environ Pollut Vol. 164, pp.89–101

Zhang, P., Imhoff, M., Wolfe, R., and Bounoua, L. 2010. Characterizing urban heat islands of global settlements using MODIS and nighttime lights products. Canadian Journal of Remote Sensing, Vol. 36, No. 3, pp. 185-196. doi: 10.5589/m10-039.

Zhang, P., Imhoff, M., Bounoua, L., and Wolfe, R. 2012. Exploring the influence of impervious surface density and shape on urban heat islands in the northeast Untied States using MODIS and Landsat. Canadian Journal of Remote Sensing, Vol. 38, No. 4, pp. 441-451.

Zhang, P., Bounoua, L., Imhoff, M. L., Wolfe, R. E., & Thome, K. 2014. Comparison of MODIS Land Surface Temperature and Air Temperature over the Continental USA Meteorological Stations. *Canadian Journal of Remote Sensing*, Vol. 40, No.2, pp.110-122.

Zhao, M., S. W. Running, *and* R. R. Nemani, 2006. Sensitivity of Moderate Resolution Imaging Spectroradiometer (MODIS) terrestrial primary production to the accuracy of meteorological reanalyses, *J. Geophys. Res.*, Vol. 111, *G01002, doi:*10.1029/2004JG000004.

Zhao, M., and S. W. Running, 2010. Drought-induced reduction in global terrestrial net primary production from 2000 through 2009. *Science*, Vol.329, pp.940–943.

Table 1: Land Cover distribution (%) and annual Gross Primary Production over the CONUS for each LC class and LC group.

LC name	Fraction of LC (%)	SiB2 GPP (Pg)	Fraction of SiB2 GPP (%)	MODIS GPP (Pg)	Fraction of MODIS GPP (%)
Broadleaf Evergreen	0.3	0.04	0.50	0.05	0.80
Broadleaf Deciduous	6.67	0.78	10.97	0.66	10.50
Mixed Forest	6.56	0.59	8.28	0.75	11.93
Needleleaf Evergreen	4.83	0.34	4.84	0.44	7.00
Needleleaf Deciduous	0.03	0.002	0.03	0.002	0.03
Savanna	8.02	0.86	12.15	0.65	10.34
Grassland	28.13	1.58	22.19	1.05	16.71
Shrubland	10.82	0.15	2.13	0.26	4.14
Barren	1.48	0.02	0.31	0.06	0.95
Cropland	32.1	2.74	38.55	2.36	37.56
Urban	1.06	0.003	0.04	0.002	0.03
Total	100	7.10	100	6.29	100

Table 2: Average summer (June-July-August) UHI of USA cities. The 300+ cities are grouped to 4 different biome types according to (Olson et al. 2001). The UHI is calculated from SiB2 simulated monthly mean ground and canopy temperatures, MODIS-Terra 8-day LST.

	SiB2 ground T	SiB2 canopy T	MODIS LST
Forest	0.91	0.62	3.58
Grass	0.55	0.58	2.17
Desert	0.62	0.80	1.14
Mediterranean	0.88	1.12	1.21

Table 3: Seasonal precipitation using North American Land Data Assimilation System (NLDAS) and surface runoff to precipitation ratio (R/P) for urban areas and rural areas grouped by four major biomes. More than 300 cities with area larger than 10 km^2 are included in this analysis.

	Forest				Grass				Mediterranean				Desert			
	Urban		Rural		Urban		Rural		Urban		Rural		Urban		Rural	
	Precipitation	R/P	Precipitation	R/P	Precipitation	R/P	Precipitation	R/P	Precipitation	R/P	Precipitation	R/P	Precipitation	R/P	Precipitation	R/P
DJF	62.89	39	61.65	12	78.06	26	77.24	8	81.20	69	80.54	17	28.51	24	28.56	5
MAM	97.58	35	96.37	15	82.20	41	80.83	25	27.08	45	27.44	25	33.37	20	33.37	9
JJA	117.66	39	116.88	23	77.28	70	75.99	49	6.03	50	4.66	38	38.43	30	37.20	14
SON	77.00	50	74.99	26	75.39	52	75.11	32	29.70	66	29.98	37	22.26	83	21.57	28

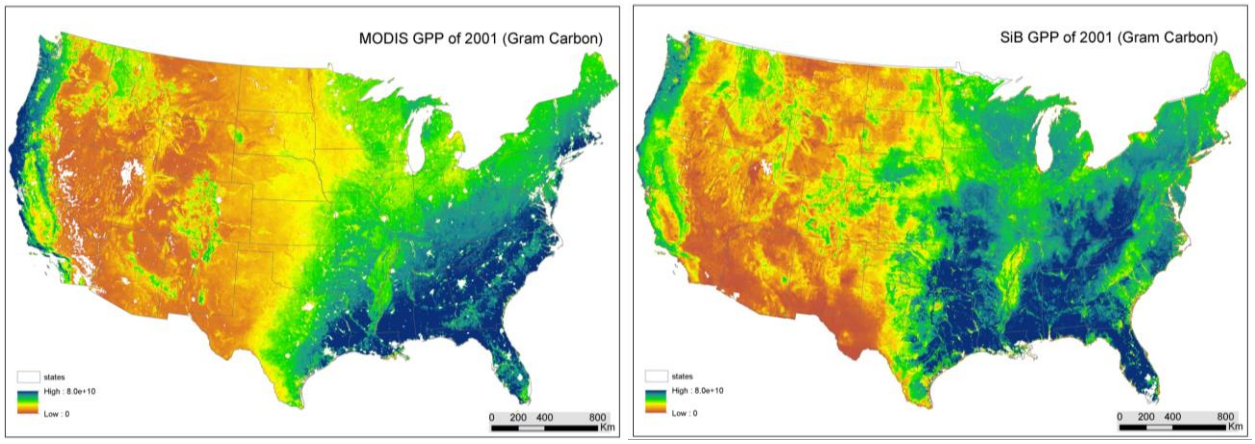

Figure 1: MODIS GPP and SiB2 model GPP of USA in 2001 in gram carbon. The 1 km MODIS GPP from NTSG group is aggregated to 0.05 degree for comparison.

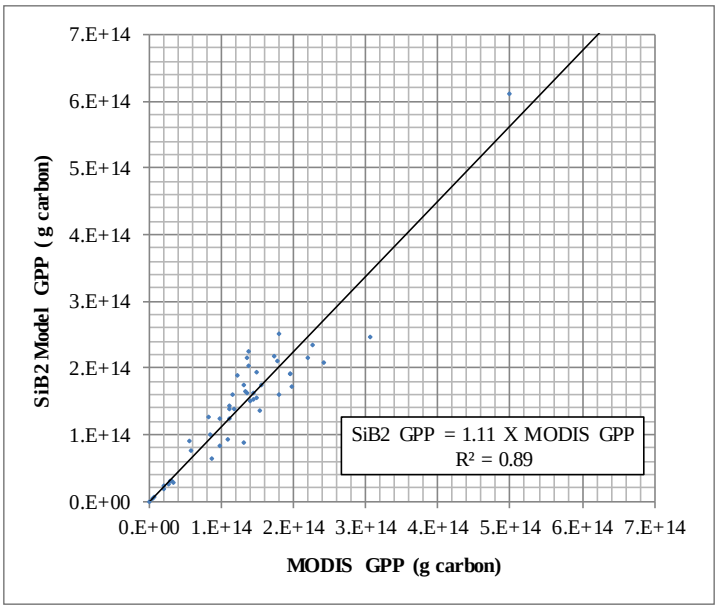

Figure 2: The relationship between MODIS GPP and SiB2 output GPP at each state for CONUS (excludes Hawaii and Alaska).

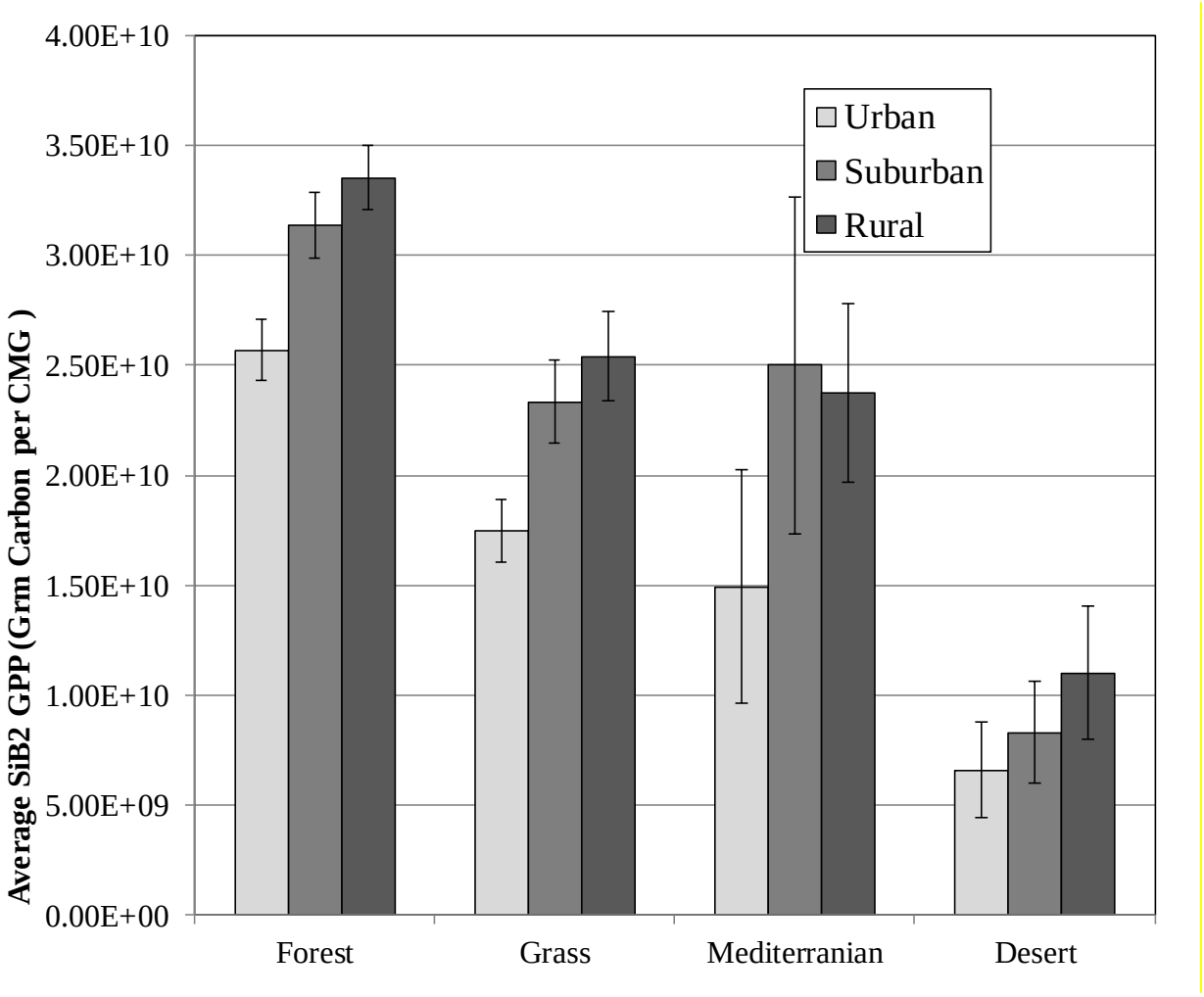

Figure 3: Average SiB_2 GPP (with 95% confidence interval) at urban, suburban, and rural zones for more than 300 cities in the CONUS. Cities are grouped by biomes defined by (Olson et al. 2001). Urban area is defined by 25% NLCD ISA contour. The Suburban area is a 5km wide ring outside the urban area and the rural area is defined by a 5km wide ring, 15-20km away from the urban (25% contour).

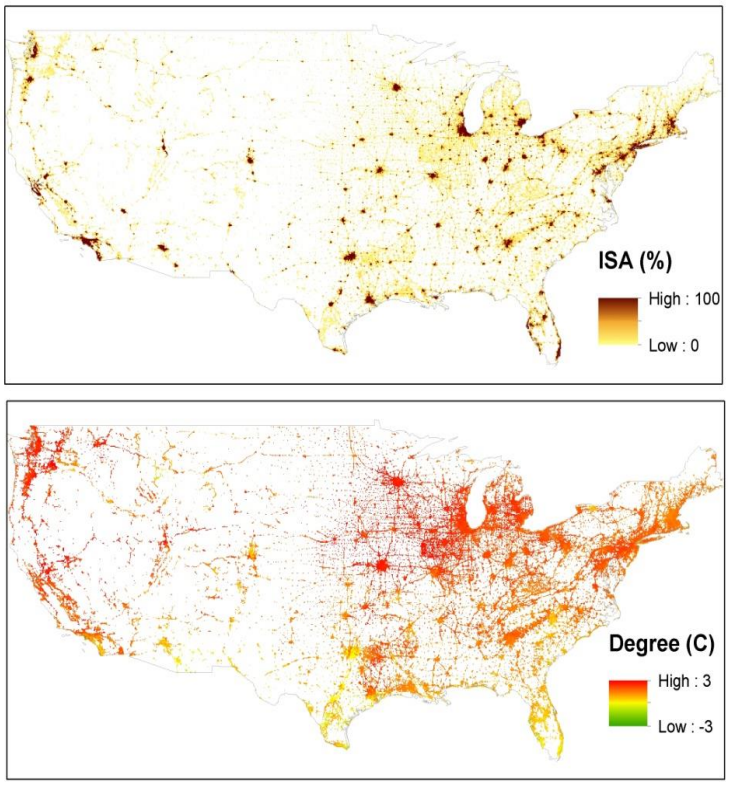

Figure 4: Temperature difference between impervious surface area and vegetated land cover types co-existing in the CMGs. Top panel shows the ISA distribution over the CONUS. Bottom panel shows the averaged summer (June-July-August) SiB2 modeled canopy temperature difference between ISA and weighted vegetated land cover types in each CMG. Only CMG with ISA larger than 1% are included in this analysis (see text for details)

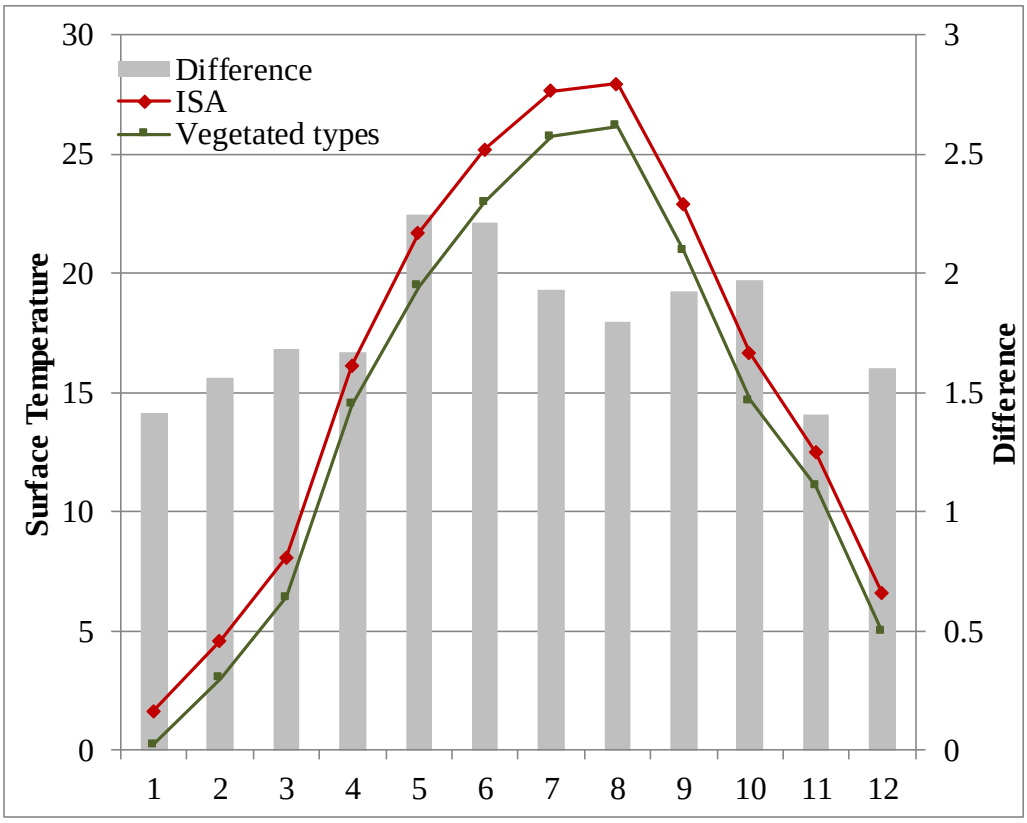

Figure 5: Annual average SiB2 modeled canopy temperature (left axis) for impervious surface area (red color) and the weighted vegetated land covers (green color) for all the ISA CMGs in USA. The average temperature difference is shown in grey bars (right axis).

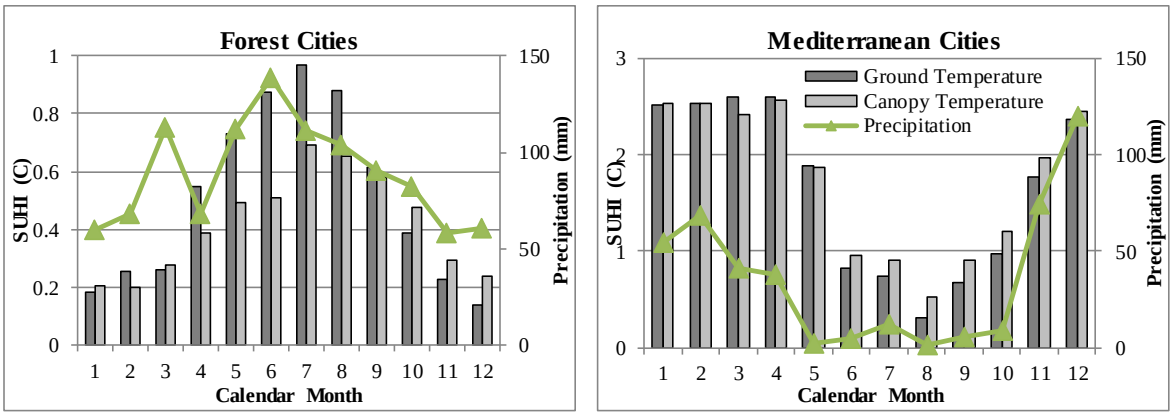

Figure 6: Monthly average surface UHI (SUHI) between urban centers and surrounding rurals for cities built in forest and Mediterranean biomes in Celsius (left axis). SUHIs from both ground and canopy temperatures are shown in dark and light grey bars, respectively. The monthly North American Land Data Assimilation System (NLDAS) precipitation is also shown as a green solid line (right axis).

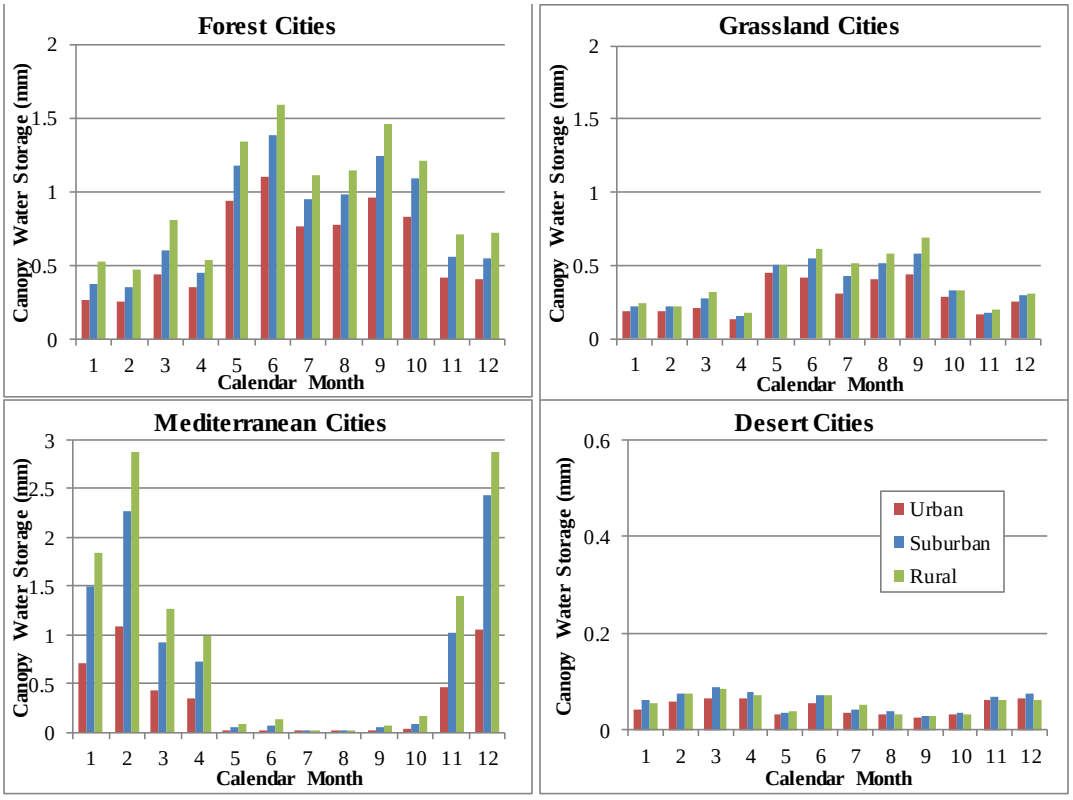

Figure 7: Monthly average SiB2 modeled canopy water storage at urban (red), suburban (blue), and rural area (green) grouped by biomes.